Earth and Planetary Science Letters 292 (2010) 191–200

Contents lists available at ScienceDirect

Earth and Planetary Science Letters

journal homepage: www.elsevier.com/locate/epsl

Magnetic mineral dissolution in Pleistocene fluvio-lacustrine sediments, Nihewan Basin (North China)

Hong Ao [a,b,c,*], Chenglong Deng [a], Mark J. Dekkers [d], Qingsong Liu [a]

[a] Paleomagnetism and Geochronology Laboratory (SKL-LE), Institute of Geology and Geophysics, Chinese Academy of Sciences, Beijing 100029, China
[b] Key Laboratory of Loess and Quaternary Geology, Institute of Earth Environment, Chinese Academy of Sciences, Xian 710075, China
[c] Graduate University of Chinese Academy of Sciences, Beijing 100049, China
[d] Paleomagnetic Laboratory 'Fort Hoofddijk', Department of Earth Sciences, Faculty of Geosciences, Utrecht University, Budapestlaan 17, 3584 CD Utrecht, The Netherlands

ARTICLE INFO

Article history:
Received 26 August 2009
Received in revised form 1 December 2009
Accepted 21 January 2010
Available online 13 February 2010

Editor: P. DeMenocal

Keywords:
environmental magnetism
dissolution
Nihewan Basin
Pleistocene
fluvio-lacustrine sediment

ABSTRACT

The Nihewan fluvio-lacustrine sequence (North China) has recorded late Pliocene–Pleistocene climatic and environmental changes, and contains valuable information on early human evolution in high-latitude East Asia. We carried out a combined mineral-magnetic and geochemical investigation on a sequence from the Xiantai section, eastern Nihewan Basin. Results suggest that large-amplitude magnetic-property variations between so-called 'high-magnetic' and 'low-magnetic' units mainly result from preservation/dissolution cycles of detrital magnetic minerals in alternating oxic and anoxic depositional environments. In our preservation/dissolution model, the high- and low-magnetic units represent glacial and interglacial deposits, respectively. This contributes to a better understanding of the link between magnetic properties and climate in the Xiantai fluvio-lacustrine sequence. Based upon this relationship, early humans may have occupied the Xiantai and Xiaochangliang sites during an interglacial period, during both interglacial and glacial periods at the Donggutuo site, and during a glacial period at the Maliang site. Our work provides a paleoenvironmental context for early human adaptation and occupation in mainland East Asia during the early Pleistocene.

1. Introduction

The Nihewan Basin is an inland basin between the North China Plain and the Inner Mongolian Plateau, ~200 km west of Beijing, which covers ~200 km^2 area (Fig. 1). It was a center of early human occupation in East Asia. Most early Pleistocene hominin or Paleolithic sites in mainland East Asia come from this basin, with ages spanning from ~1.7 Ma to at least ~0.8 Ma (see reviews by Zhu et al. (2007)). Thus, knowledge of Pleistocene climatic and environmental conditions and their fluctuations in this area is critical for investigating early human adaptation and occupation in East Asia. Such knowledge may provide explanation(s) for human adaptation and, possibly, boundary conditions for human settlement. However, the climatic context of the Paleolithic sites in the basin is presently poorly resolved, although several paleoclimatic records have been retrieved from this area (e.g. Li et al., 2008; Wang et al., 2008; Ao et al., 2009). For example, it is not yet clear whether human occupation occurred during interglacial and/or glacial periods.

Since the development of environmental magnetism with the study of lake sediments in the 1970s (Thompson et al., 1980), it has been successfully adopted in reconstructing the climatic and environmental evolution of marine and continental sediments (e.g. Evans and Heller, 2003). Two recent investigations indicate that magnetic and bulk grain-size parameters for the Nihewan fluvio-lacustrine sediments are closely related to glacial/interglacial cycles expressed in the marine oxygen isotope record (Li et al., 2008; Wang et al., 2008). However, the mechanism of how magnetic properties responded to the changing environment and climate remains poorly understood, and the high-magnetic units are correlated to interglacial periods by Wang et al. (2008) and to glacial periods by Li et al. (2008), respectively. Thus we have carried out a combined magnetic and geochemical investigation on this sedimentary sequence to test these interpretations and to identify the mechanism for the magnetic property–climate relationship. We also discuss the relationship between magnetic properties and climate and its implications for early human occupation.

2. Study section

The Xiantai (40°13.126′ N, 114°39.623′ E; also named Dachangliang (Pei, 2002)) section is located at the eastern margin of the Nihewan Basin (Fig. 1c). Here, the fluvio-lacustrine sequence has a thickness of 64.5 m. It mainly consists of grayish-green silts/clays and grayish-yellow

* Corresponding author. Key Laboratory of Loess and Quaternary Geology, Institute of Earth Environment, Chinese Academy of Sciences, Xian 710075, China. Tel.: +86 29 88329660.
E-mail addresses: aohong@ieecas.cn (H. Ao), cldeng@mail.igcas.ac.cn (C. Deng), dekkers@geo.uu.nl (M.J. Dekkers), liux0272@yahoo.com (Q. Liu).

0012-821X/$ – see front matter © 2010 Elsevier B.V. All rights reserved.
doi:10.1016/j.epsl.2010.01.035

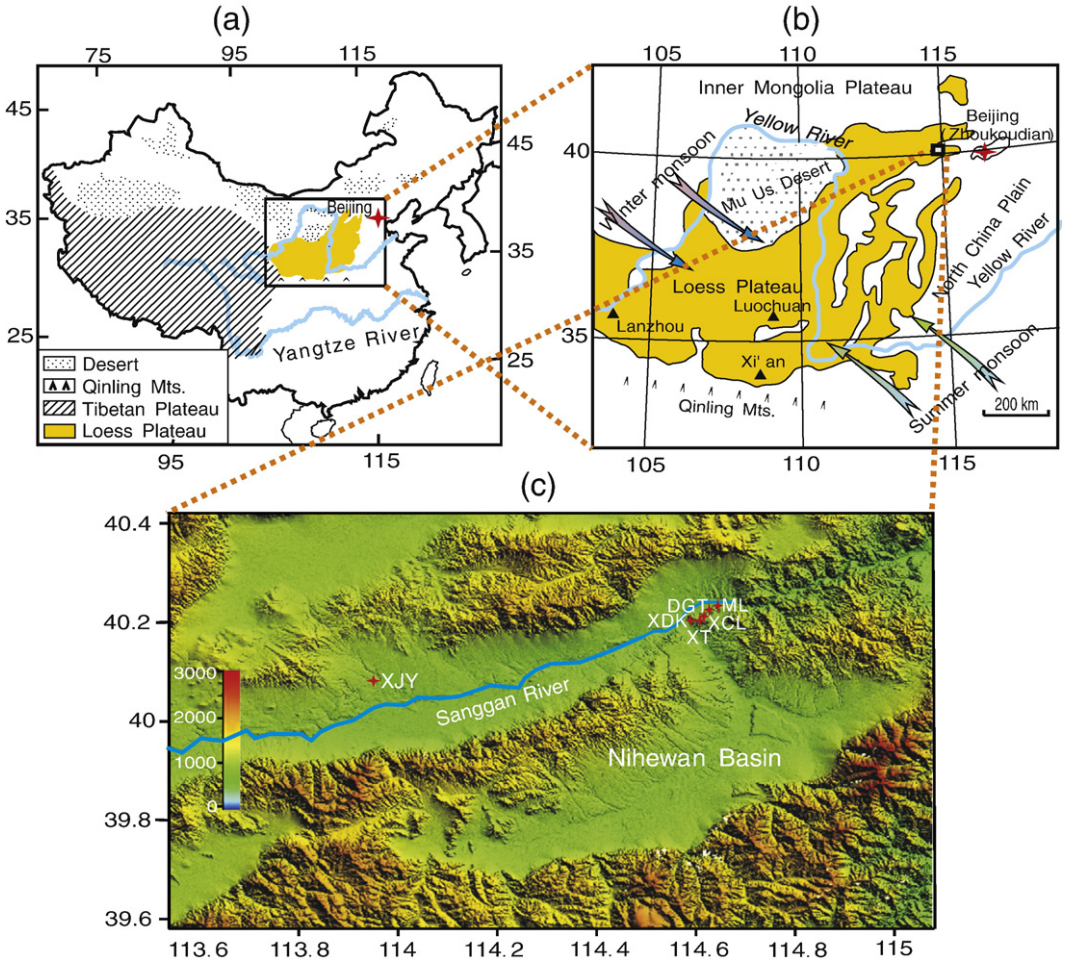

Fig. 1. Topographic location map for the Nihewan Basin. The Yellow River and Yangtze River are the major river systems in north and south China, respectively. The east–west trending Qinling Mountains are the traditional dividing line between temperate northern China and subtropical southern China. The arrows show the summer or winter monsoon directions. XT, Xiantai; XCL, Xiaochangliang; DGT, Donggutuo; ML, Maliang; XDK, Xiaodukou; XJY, Xujiayao.

silts/clays with some intercalated fine-grained sand layers (Fig. 2a). The grayish-green silt/clay units generally have low-magnetic susceptibility (χ, 1×10^{-8} m^3/kg$<\chi<30\times10^{-8}$ m^3/kg) and have laminated and fine planar textures with a small coarse-grained fraction, which suggests deposition under relatively deep, perennial lake conditions. In contrast, the grayish-yellow silt/clay and fine-grained sand units generally have high χ (30×10^{-8} m^3/kg$<\chi<300\times10^{-8}$ m^3/kg) and larger coarse-grained fraction without laminated and fine planar textures, which suggests relatively shallow depositional conditions in oxic lake water. However, this is not a uniform pattern. There are a few intervals where grayish-green silts/clays have high χ values, and grayish-yellow silts/clays have low χ values. This implies that magnetic parameters may indicate more subtle lithological variations than color.

The Xiantai fluvio-lacustrine sequence ranges from early Olduvai to late Brunhes in age, as established by magnetostratigraphy (Deng et al., 2006). For magnetostratigraphic study, 196 oriented block samples were collected with a spacing of 20–40 cm (Deng et al., 2006). Here, all the 196 unheated left-overs of those samples were used for environmental magnetic analyses. An age model was developed by linear interpolation between geomagnetic event/reversal age tie points (Ao et al., 2009).

3. Methods

An anhysteretic remanent magnetization (ARM) was imparted using a 100 mT alternating field (AF) and a 0.05 mT direct current (DC) bias field. The ARM was expressed in terms of the ARM susceptibility (χ_{ARM}), which was obtained by dividing the ARM intensity by the DC field strength. Isothermal remanent magnetizations, acquired in inducing fields of 0.3 T (hereafter termed $IRM_{0.3\,T}$) and 1 T (IRM_{1T}), were used to calculate the forward S*-ratio (S*-ratio $= IRM_{0.3\,T}/IRM_{1T}$), which reflects the relative content of low to high coercivity magnetic minerals. HIRM*, which is defined as ($IRM_{1T} - IRM_{0.3\,T}$), was used to quantify the absolute concentration of hematite. The IRM_{1T} was further demagnetized in a 100 mT AF to calculate the *L*-ratio (*L*-ratio $=$ HIRM*/$IRM_{1T,\,AF@100mT}$; where $IRM_{1T,\,AF@100mT}$ represents the residual IRM_{1T} after AF demagnetization at 100 mT). The *L*-ratio enables characterization of coercivity variations in the high-coercivity component (e.g. hematite) for samples with mixed magnetic mineralogy (e.g. mixtures of magnetite and hematite) (Liu et al., 2007). Since natural hematite dominantly occurs in the stable single-domain (SD) range, its coercivity is positively correlated to grain size (Chevallier and Mathieu, 1943). Thus for the Nihewan sediments *L*-ratio positively correlated to hematite grain-size variations. Magnetic remanence was measured using a 2-G Enterprises Model 760-R cryogenic magnetometer housed in a magnetically shielded space (<300 nT).

Magnetic hysteresis parameters, including the saturation magnetization (M_s), saturation remanence (M_{rs}), coercive force (B_c), coercivity of remanence (B_{cr}), IRM acquisition curves, and first-order reversal curve (FORC) diagrams were measured on a Princeton Measurements Corp. Model 2900 MicroMag alternating gradient magnetometer (AGM). The maximum applied field was 1 T. Paramagnetic

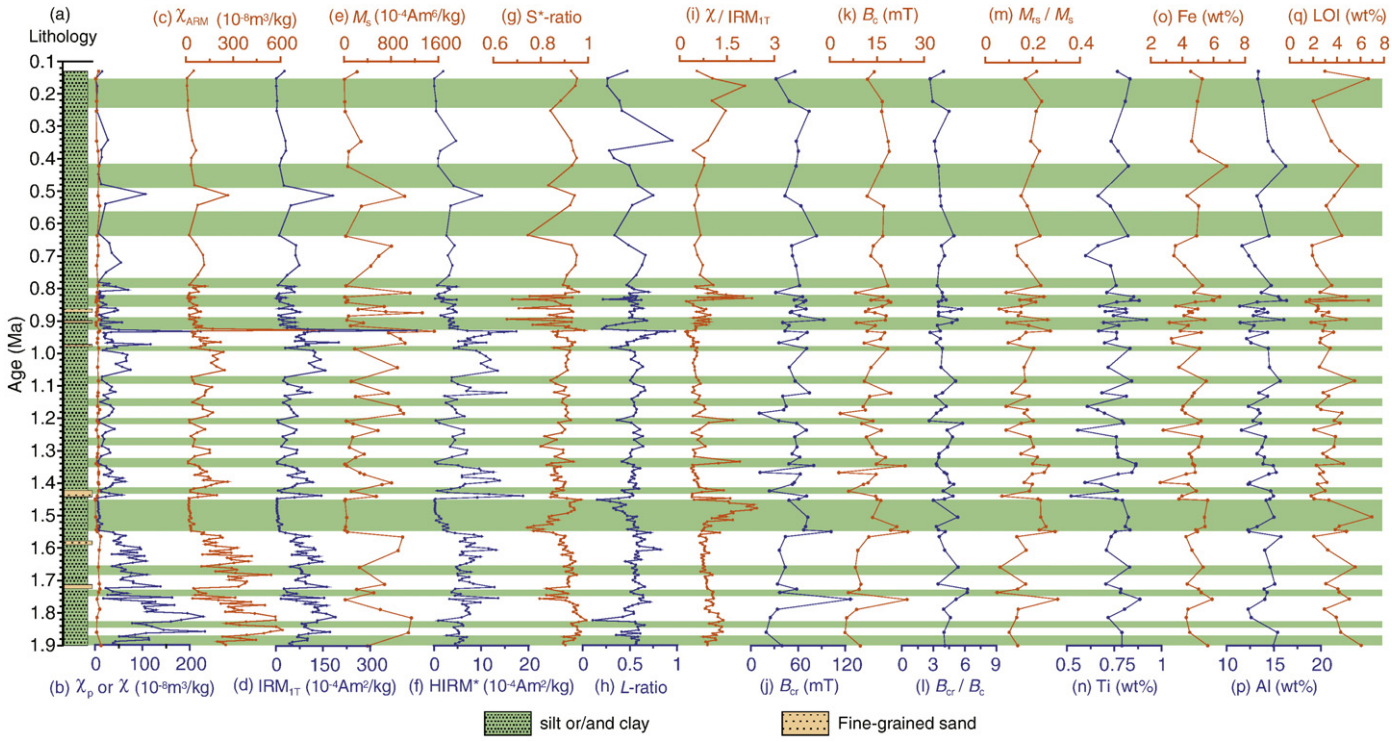

Fig. 2. (a) Lithostratigraphy (Deng et al., 2006), (b) paramagnetic susceptibility (χ_p, orange line) and magnetic susceptibility (χ, blue line) (Ao et al., 2009), (c) χ_{ARM}, (d) IRM_{1T}, (e) M_s, (f) HIRM*, (g) S^*-ratio, (h) L-ratio, (i) χ/IRM_{1T}, (j) B_{cr}, (k) B_c, (l) B_{cr}/B_c, (m) M_{rs}/M_s, (n) Ti, (o) Fe, (p) Al and (q) LOI of the Xiantai fluvio-lacustrine sequence. The green shadings represent the low-magnetic units.

susceptibility χ_p was calculated from the slope of the hysteresis loops between 800 and 1000 mT. For each sample, 125 FORCs were measured with fields up to 1 T, and data were processed using the *FORClab* software with a smoothing factor (SF) of 4 (Roberts et al., 2000).

Temperature-dependent susceptibility (χ–T) curves were measured in an argon atmosphere (with a flow rate of 100 ml/min) at a frequency of 875 Hz from room temperature up to 700 °C and back to room temperature using a KappaBridge magnetic susceptibility meter (model KLY-3) equipped with a CS-3 high-temperature furnace (AGICO Ltd., Brno, Czech Republic). Low-temperature magnetic measurements were performed on a Quantum Designs superconducting quantum interference device (SQUID) Magnetic Properties Measurement System (MPMS). An IRM acquired in a 5 T field at 5 K (hereafter termed $IRM_{5T@5\ K}$) after zero field cooling (ZFC) was measured during warming from 5 to 300 K. This was followed by cooling in a 5 T field (FC) from 300 to 5 K after which the resulting IRM was measured during warming from 5 to 300 K. Finally, the IRM acquired in 5 T at 300 K (hereafter termed $IRM_{5T@300\ K}$) was measured from 300 to 5 K. The low-temperature susceptibility was measured from 5 to 300 K at two frequencies, 1 and 1000 Hz. Its frequency dependence for each temperature (χ_{fd}–T) is defined as $\chi_{fd} = \chi_{1Hz} - \chi_{1000Hz}$.

X-ray fluorescence (XRF) analyses for Ti, Fe and Al concentrations were measured on a Shimadzu XRF-1500 spectrometer. The Ti- and Al-bearing oxides and sphene are not significantly affected by dissolution under most post-depositional conditions, thus variations in Ti and Al can be used to assess variations in detrital mineral inputs (including detrital magnetic minerals) during deposition (Rosenbaum et al., 1996; Ortega et al., 2006). In contrast, iron oxides (when unsubstituted) and iron oxide coatings around silicates are relatively unstable and can undergo alteration under some post-depositional conditions (Rosenbaum et al., 1996). Comparing these major elements with the magnetic properties therefore provides elucidation of the detrital magnetic signal and post-depositional alteration.

Loss on ignition (LOI, expressed as a percentage; here we use an ignition temperature of 550 °C) is a rapid method for estimating the organic carbon content. LOI was determined by weighing samples after oven-drying at 110 °C for 4 h, annealing at 550 °C for 3 h, followed by reweighing (Beaudoin, 2003).

To further characterize the magnetic mineralogy and to trace pyrite as an indicator of anoxic conditions, manually prepared magnetic extracts were made from sample DCL050 (from a high-magnetic unit) and sample DCL028 (from a low-magnetic unit) with a rare-earth magnet. X-ray diffraction (XRD) analysis of the extracts was carried out using an X'Pert Pro MPD X-ray diffractometer with the following parameters: Cu-Kα/40 kV/40 mA, divergence slit of 0.5°, scattering slit of 1°, receiving slit of 0.3 mm, continuous scan mode, scanning speed of 2.5° 2θ/min and a scan step of 0.02° 2θ.

4. Magnetic and geochemical data

The high- and low-magnetic units are defined by broad variations in χ, χ_{ARM}, IRM_{1T} and M_s (Fig. 2b–e). Consistent variations in χ, χ_{ARM}, IRM_{1T} and M_s indicate that their variations are mainly controlled by changes in magnetite concentration rather than by grain-size variation. At the bottom of the section (from ~1.9 to ~1.6 Ma), variable magnetite concentration and high-frequency variations suggested by χ and χ_{ARM} (Fig. 2b, c) are interpreted to indicate an interval of intense catchment erosion, with high sedimentation rates during the initiation of lake sediment deposition. This interpretation is consistent with the lithology in this interval, which contains a large amount of coarse littoral deposits intercalated with conglomerates. From ~1.6 to 1.0 Ma the expression of the variability is typical for the section. From ~1 to 0.8 Ma, the resolution in time increases slightly, because of a somewhat higher sedimentation rate. Above 0.8 Ma the resolution in time decreases substantially, because the sedimentation rate decreased.

Stratigraphic changes in hematite content (HIRM*), as well as in the relative percentage of magnetite to hematite (S*-ratio), are generally in phase with changes in magnetite content over both long and short time scales (Fig. 2f, g). Two exceptions are observed: (1) at the bottom of the section (from ~1.9 to ~1.6 Ma), decreasing magnetite contents (χ and χ_{ARM}) correspond to increasing hematite contents (HIRM*); and (2) the upper part of a low-magnetic unit (from ~1.49 to ~1.45 Ma) has low χ, χ_{ARM}, IRM_{1T}, M_s and HIRM* values but high S*-ratios. In addition, high-magnetic units generally have higher *L*-ratios than low-magnetic units (Fig. 2h), which indicates lower hematite coercivities and thus a smaller average hematite grain size in the low-magnetic units (Liu et al., 2007). High-magnetic units generally have lower χ/IRM_{1T}, B_{cr}, B_c and M_{rs}/M_s values and higher B_{cr}/B_c values than low-magnetic units (Fig. 2i–m), which implies a relatively larger average magnetic grain size in the former.

Stratigraphic changes in Ti, Fe and Al contents have an opposite relationship with changes in magnetic mineral concentration, with lower values in the high-magnetic units (Fig. 2n–p), which suggests a lower detrital input (including detrital magnetic minerals) in these units. In addition, samples from high-magnetic units generally have lower organic contents as indicated by lower LOI values (Fig. 2q).

The entire χ data set has a strong positive correlation with χ_{ARM} ($R=0.95$) and M_s ($R=0.87$) (Supplementary Fig. 1a, b). A similarly high correlation between M_s and M_{rs} is also observed (Supplementary Fig. 1c). This confirms that magnetic mineral concentration (rather than magnetic grain size) is largely indicated by these parameters. HIRM* is positively correlated with χ and χ_{ARM}, and negatively correlated with the S*-ratio for the low-magnetic unit samples, whereas data from high-magnetic units are scattered (Fig. 3a–c). Furthermore, the low-magnetic units have a larger variation in their S*-ratios than the high-magnetic units (Fig. 3c). For the high-magnetic units, the *L*-ratio appears to be independent of HIRM*, while there is a positive correlation between the *L*-ratio and HIRM* for the low-magnetic units (Fig. 3d). The positive correlation between the *L*-ratio and HIRM* indicates a decreasing hematite concentration with decreasing grain size in the low-magnetic units. Positive correlation is observed between χ and χ/IRM_{1T} for the high-magnetic units, which suggests that their magnetite concentration and grain size generally increase and decrease synchronously; such a relationship is not observed for the low-magnetic units (Fig. 3e). In addition, for the high-magnetic units, there appears to be a positive linear relationship between M_s and Ti; the low-magnetic units do not have such a relationship (Fig. 3f).

The X-ray diffractograms reveal the presence of magnetite in the magnetic extracts from both low- and high-magnetic unit samples (Fig. 4). Pyrite, an important paramagnetic mineral indicating anoxic conditions, is only found in the extract from the low-magnetic unit sample.

5. Magnetic mineralogy

Detailed rock magnetic analyses (χ–T curves, low-temperature magnetic measurements, IRM acquisition and magnetic hysteresis measurements) were carried on 72 selected samples from different stratigraphic intervals that are characterized by χ maxima and minima. This reveals in detail differences in magnetic mineral concentration, composition and grain size from high- and low-magnetic units. Such a multi-parameter approach enabled better interpretation of changes in rock magnetic properties and thus better understanding of their link with climatic and environmental changes.

5.1. χ–T curves

Each of the χ–T heating curves undergoes a marked decrease near 580 °C, which suggests the ubiquitous occurrence of magnetite in the

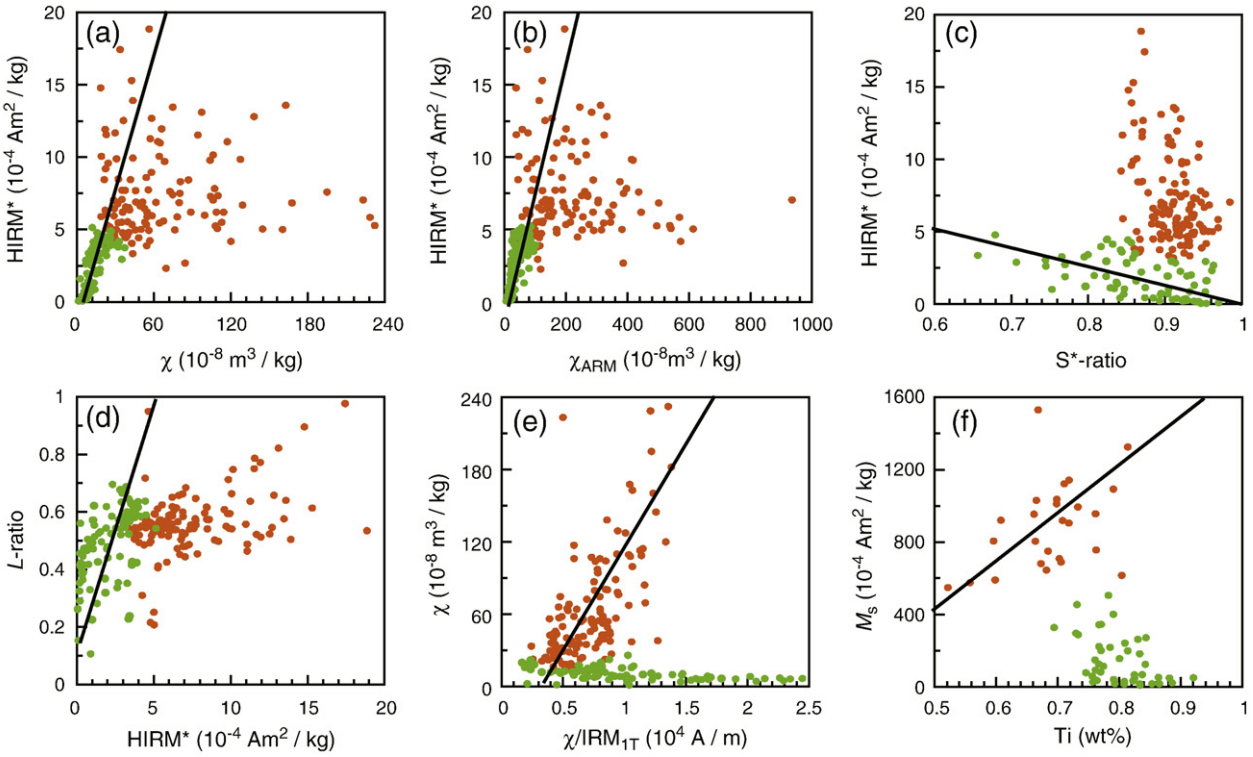

Fig. 3. (a) HIRM* versus χ, (b) HIRM* versus χ_{ARM}, (c) HIRM* versus S*-ratio, (d) *L*-ratio versus HIRM*, (e) χ versus χ/IRM_{1T}, and (f) M_s versus Ti for the Xiantai fluvio-lacustrine sequence. Orange and green circles represent data from high- and low-magnetic units, respectively. In (a–d) the linear trends between the magnetic parameters for low-magnetic units suggest that their magnetic mineralogy is controlled by dissolution. In (e–f) the linear trends between the magnetic parameters from high-magnetic units suggest that their magnetic mineralogy is controlled by detrital input rather than by dissolution.

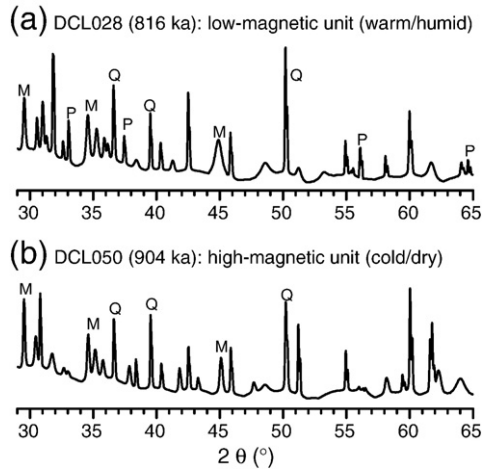

Fig. 4. X-ray diffractograms of magnetic extracts from (a) low-magnetic unit sample DCL028 and (b) high-magnetic unit sample DCL050 from the Xiantai fluvio-lacustrine sequence. Both magnetite and pyrite are shown to occur in sample DCL028, while only magnetite (without pyrite) is shown to occur in sample DCL050. Quartz appears to be still present in the magnetic concentrates. M, magnetite; P, pyrite; Q, quartz.

sediments (Fig. 5). χ increases during cooling after heating to 700 °C are interpreted to result from the neoformation of fine-grained magnetite via annealing of iron-containing paramagnetic chlorite (Ao et al., 2009). The high-magnetic unit samples usually undergo a χ drop between ~300 and ~400 °C (Fig. 5a–c), which results from conversion of metastable maghemite to weakly magnetic hematite. This χ drop is relatively weak or absent in the low-magnetic unit samples (Fig. 5d–f), which suggests that their maghemite concentrations are not significant.

5.2. Low-temperature magnetic data

Consistent with the presence of a high magnetite content, high-magnetic unit sample DCL056 has a clear Verwey transition at ~110 K (Fig. 6a). Furthermore, frequency-dependence of χ between ~50 and 300 K, with higher values at 1 Hz (Fig. 6a), suggests the presence of superparamagnetic (SP) particles. The χ_{fd} peak between 30 and 80 K (Fig. 6b) could be caused by either or both relaxation of SP magnetite particles and domain walls associated with multidomain (MD) magnetite particles (Moskowitz et al., 1993, 1998; Kosterov, 2003). Both χ and χ_{fd} undergo a quasi-linear increase when warming above 120 K, which suggests a relatively broad grain-size distribution, possibly from SP to MD (Worm, 1998). The sharp decrease in χ and remanence during warming from 5 to 50 K (Fig. 6a–c) may relate to the presence of SP particles and paramagnetic minerals (Coey, 1988; Dunlop and Özdemir, 1997). Magnetic interaction and surface effects in very fine particles (Pike et al., 2000; Passier and Dekkers, 2002) can also play a role. Warming of $IRM_{5T@5K}$ after ZFC and FC indicates a barely visible Verwey transition (Fig. 6c). A broad maximum in the $IRM_{5T@300K}$ cooling curve is also observed at ~230 K. Upon continued cooling, however, the remanence decays almost linearly to 5 K without a change in slope at the Verwey transition temperature.

Low-magnetic unit sample DCL017 has no frequency-dependence of χ at low temperature (Fig. 6d). Neither χ nor χ_{fd} has a quasi-linear increase above 120 K (Fig. 6d, e). These characteristics indicate a relatively narrow grain-size distribution of magnetite (Worm, 1998), with only marginal occurrence of SP and MD particles (Moskowitz et al., 1993, 1998; Kosterov, 2003). Neither χ nor remanence warming curves has a recognizable Verwey transition (Fig. 6d, f), which is consistent with its low magnetite content. The $IRM_{5T@300K}$ cooling curve has a quasi-linear increase down to ~50 K; however, upon continued cooling to 5 K, the remanence decreased sharply and linearly (Fig. 6f). Since fine-grained oxide particles are insignificant in

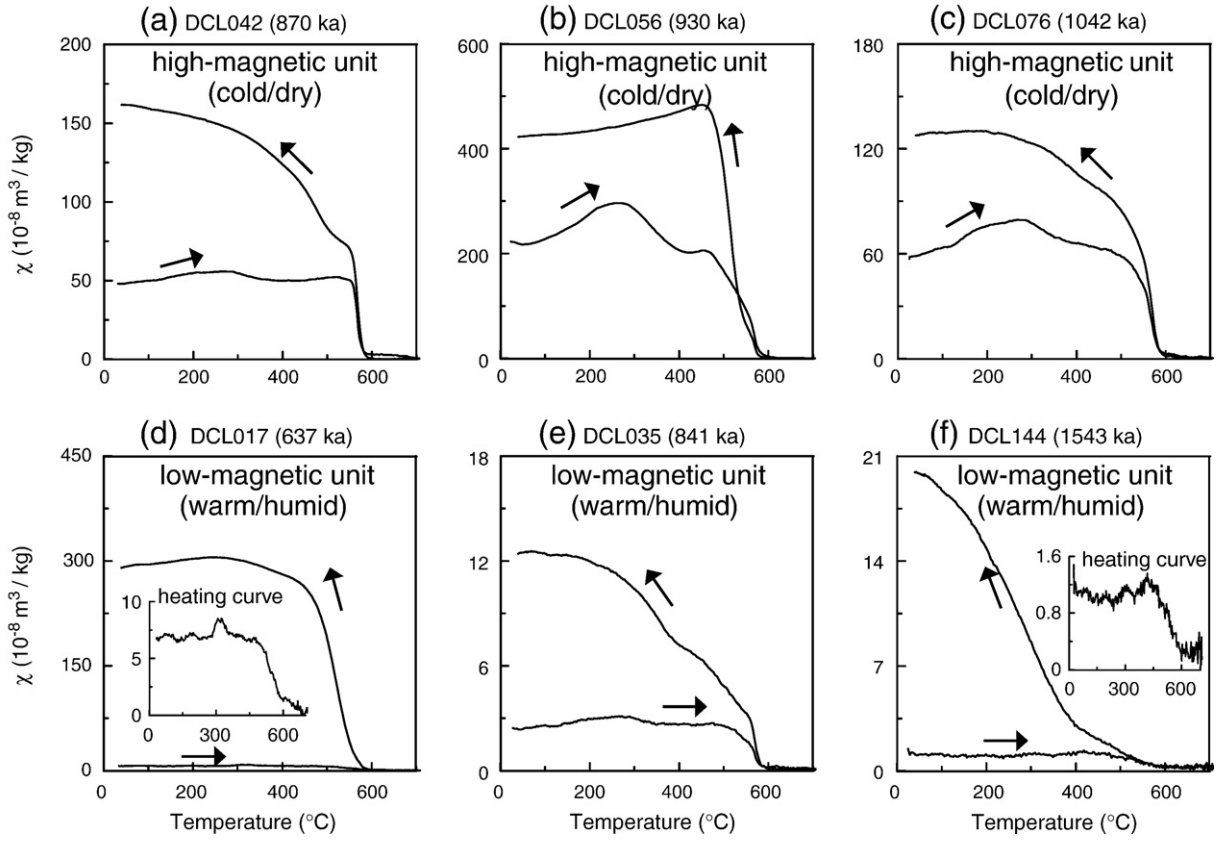

Fig. 5. χ–T curves for selected samples from the (a–c) high-magnetic and (d–f) low-magnetic units from the Xiantai fluvio-lacustrine sequence.

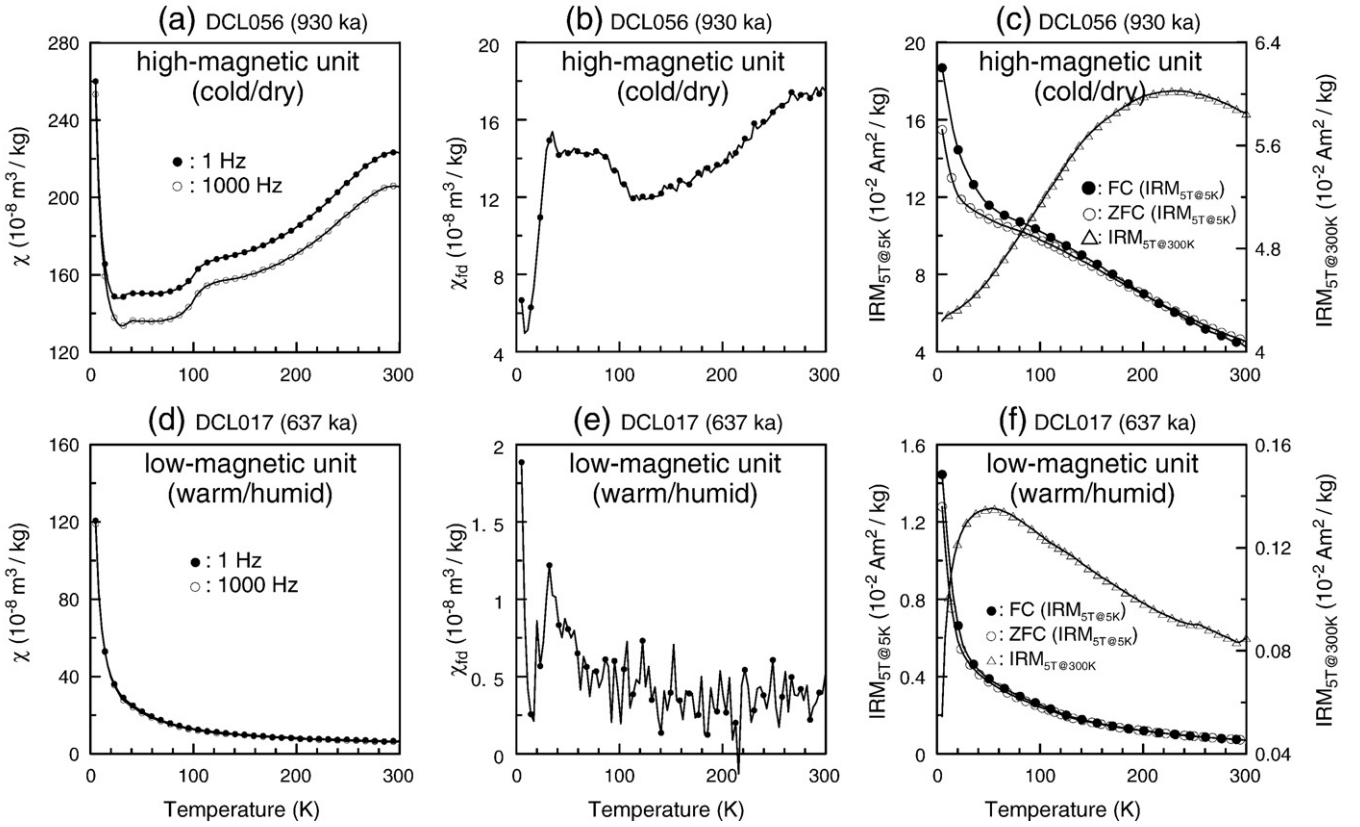

Fig. 6. Low-temperature magnetic measurements for two selected samples from (a–c) the high-magnetic and (d–f) low-magnetic units from the Xiantai fluvio-lacustrine sequence. (a, d) Frequency-dependence of magnetic susceptibility at low temperature, (b, e) low-temperature χ_{fd}–T curves and (c, f) thermal warming of $IRM_{5T@5K}$ from 5 to 300 K after cooling in zero field (ZFC) and after cooling in a 2.5 T field (FC) from 300 K and cooling of $IRM_{5T@300K}$ from 300 to 5 K.

this type of sediment, the sharp and linear changes in χ and remanence between 5 and 50 K are interpreted to be due to paramagnetic minerals (Coey, 1988).

5.3. IRM acquisition curves

IRM acquisition curves for low- and high-magnetic units have notably different behavior (Fig. 7). Samples from high-magnetic units are virtually saturated magnetically after application of a ~400 mT field, which indicates again that these samples are dominated by (partially oxidized) magnetite. However, the low-magnetic units are not saturated even at a 1000 mT field, which suggests a significant hematite contribution.

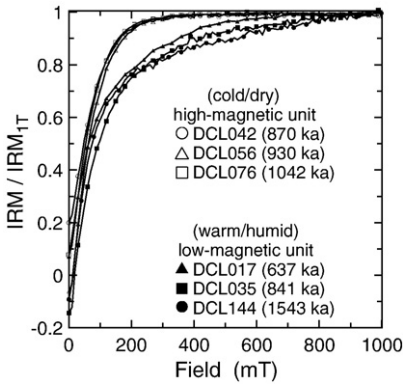

Fig. 7. Isothermal remanent magnetization acquisition curves for selected samples from the high-magnetic (open symbols) and low-magnetic (solid symbols) units of the Xiantai fluvio-lacustrine sequence. IRMs are normalized to their 1 T values.

5.4. Hysteresis properties

5.4.1. Hysteresis loops

The dominance of the magnetic properties of the high-magnetic units by magnetite is further supported by the "narrower" hysteresis loops that close below ~400 mT (Fig. 8a–c). In contrast, the low-magnetic units have strongly wasp-waisted hysteresis loops that do not close below 800 mT (Fig. 8d–f), which is consistent with mixtures of significant concentration of hematite with magnetite (Roberts et al., 1995).

5.4.2. Day plot and FORC diagrams

The ratios of M_{rs}/M_s and B_{cr}/B_c are commonly plotted on a so-called Day plot to visualize the dominant domain state of the ferrimagnetic materials (Day et al., 1977; Dunlop, 2002). The ratios for the low-magnetic units are generally located in the pseudo-single-domain (PSD) field above those from the high-magnetic units (Fig. 9e), in line with a smaller typical magnetic grain size in the former. It should be noted that the presence of hematite and SP particles may have shifted data to the right with respect to the SD + MD mixing line on a Day plot, at least to some extent (Roberts et al., 1995; Dunlop and Özdemir, 1997).

Consistent with the data distribution on the Day plot, the FORC diagrams for low- and high-magnetic units have different behavior (Fig. 9). FORC diagrams for low-magnetic unit samples DCL017, DCL035 and DCL127 are characterized by one or two closed inner contours and outer contours that diverge along the B_u axis (B_u represents the interaction field among magnetic grains). Divergence of contours along the B_u axis, however, is not large (<40 mT) (Fig. 9a–c), which indicates a dominance of PSD magnetite in these samples (Roberts et al., 2000; Muxworthy and Dunlop, 2002; Carvallo et al., 2006). Also the 'tail' of a high-coercivity contribution in the FORC

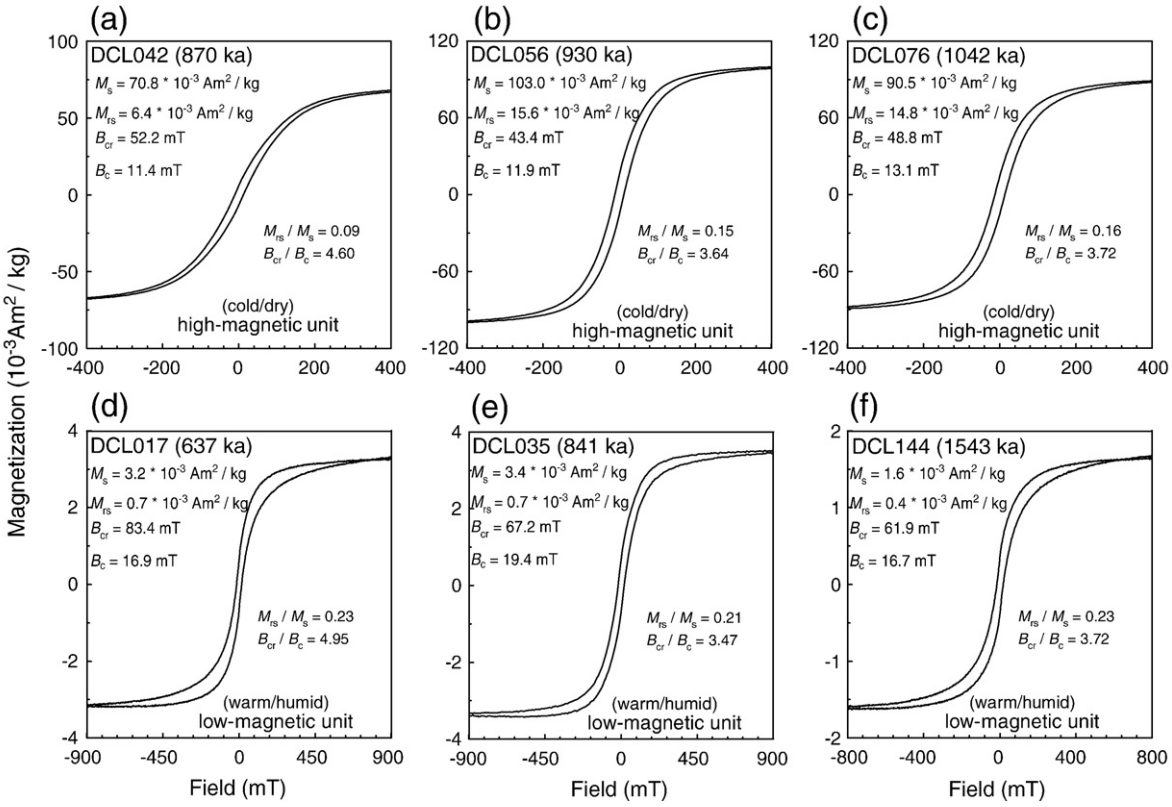

Fig. 8. Hysteresis loops for selected samples from the (a–c) high-magnetic and (d–f) low-magnetic units of the Xiantai fluvio-lacustrine sequence.

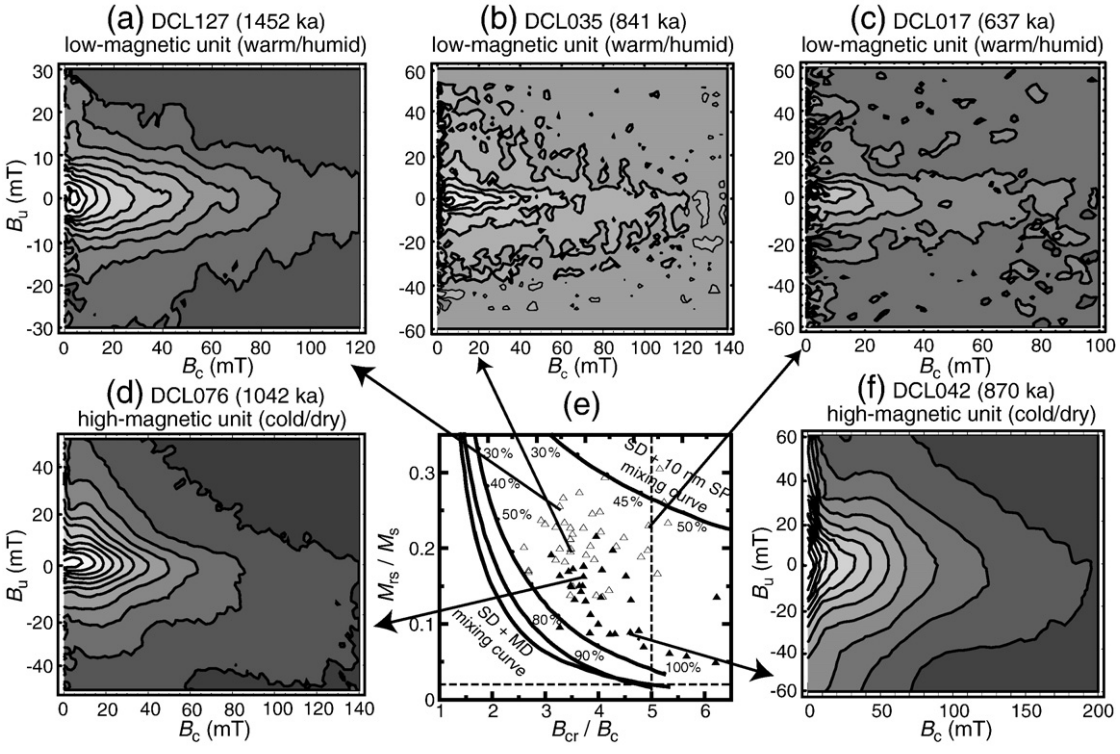

Fig. 9. FORC diagrams for selected samples from the (a–c) high-magnetic and (d, f) low-magnetic units of the Xiantai fluvio-lacustrine sequence, derived with a smoothing factor of 4 (Roberts et al., 2000). (e) Hysteresis ratios for representative samples (Ao et al., 2009) plotted on a Day plot (Day et al., 1977) with the mixing curves from Dunlop (2002). The open and solid triangles in (e) represent data from low-magnetic and high-magnetic units, respectively.

distribution is fairly prominent (on a relative basis) in these samples compatible with the presence of hematite. FORC diagrams for high-magnetic unit samples DCL076 and DCL042 are characterized by more divergent contours along the B_u axis (>60 mT) (Fig. 9d, f), which suggests the dominance of MD magnetite grains in these samples (Roberts et al., 2000; Muxworthy and Dunlop, 2002; Carvallo et al., 2006). A small high-coercivity tail hints at some hematite present (IRM acquisition curves are close to saturation but not yet entirely saturated in the maximum field of 1 T). In addition, these samples have a low coercivity peak near the origin of FORC diagram, suggesting the presence of particles near the SP/SD threshold size (Pike et al., 2001).

6. Discussion

6.1. Causes for magnetic-property variations

The combined rock magnetic analysis suggests a distinct contrast in magnetic mineral concentration, composition and grain size between samples from high- and low-magnetic units. Lower concentrations of magnetic minerals, lower relative proportions of magnetite to hematite and smaller average magnetic grain sizes are typical of the latter (Fig. 2b–m). In particular, the concentrations of magnetic minerals contrast considerably, spanning variations of over two orders of magnitude. Three scenarios are feasible to explain the low-magnetic mineral contents (as indicated by χ, χ_{ARM}, IRM_{1T} and M_s minima) in the low-magnetic units of the Nihewan fluvio-lacustrine sediments: (1) changes in provenance; (2) decrease in detrital magnetic mineral inputs; and (3) post-depositional dissolution of detrital magnetic minerals. Reasonably high correlation between Ti and Al contents ($R=0.61$) (Supplementary Fig. 2) indicates that provenance has not changed significantly, because changes in provenance that reflect differences in bedrock composition would result in significant variations in the relative concentrations of elements that are not prone to diagenetic alteration (e.g., Ti and Al). Although a decreased flux of detrital magnetic minerals into the lake can give rise to low concentrations of magnetic minerals, this is unlikely to be the cause for Nihewan. The low-magnetic units (with χ, χ_{ARM}, IRM_{1T} and M_s minima) were likely to have had relatively high detrital mineral influxes (including detrital magnetic minerals), as indicated by Ti and Al maxima (Fig. 2).

Post-depositional dissolution of detrital magnetic minerals during and after burial is common in (shallow) marine (Karlin and Levi, 1983, 1985; Karlin et al., 1987; Canfield and Berner, 1987) and lake sediments (Snowball, 1993; Rosenbaum et al., 1996; Williamson et al., 1998; Nowaczyk et al., 2001, 2002; Demory et al., 2005; Ortega et al., 2006). Dissolution tends to remove the fine-grained (SP and SD) magnetic particles first, which leads to increased detrital magnetic mineral grain sizes; more intensive and prolonged dissolution may subsequently destroy the remaining coarse-grained (MD and PSD) magnetic particles, which then results in an overall decrease of the magnetic mineral grain sizes (Karlin and Levi, 1983, 1985). Dissolution rates and effects on magnetic minerals are modulated by the availability and reactivity of both organic matters and reductants on the one hand and the competitive efficiency of microbial populations on the other (Karlin and Levi, 1983; Snowball, 1993; Tarduno, 1994; Nowaczyk et al., 2001). Thus, dissolution of magnetic minerals will differ with environment. For example, dissolution in Lake Baikal is suggested to have mainly removed fine-grained magnetite particles while leaving hematite particles virtually untouched (Demory et al., 2005), whereas intensive dissolution of hematite is reported for Lake Tritrivakely, Madagascar (Williamson et al., 1998). Diagenetic reactions can proceed in both steady-state and non-steady-state regimes in relation to changing accumulation and degradation rates of organic matter (Thouveny et al., 1994; Williams et al., 1996; Williamson et al., 1998; Larrasoaña et al., 2003a). In addition, dissolution of magnetic minerals and iron oxide coating around silicates provides Fe, which then can react with other dissolved elements and subsequently yield new minerals. The neoformation of ferrimagnetic minerals (e.g. SP greigite) would result in magnetic enhancement (Tarduno, 1995; Rowan and Roberts, 2006; Rowan et al., 2009).

Post-depositional dissolution of detrital magnetic minerals in the Nihewan fluvio-lacustrine sequence is suggested by rock magnetic and geochemical data. First, χ values for the low-magnetic units are as low as their χ_p values (Fig. 2b), which suggests that most magnetite particles have been removed. Second, most low-magnetic units were deposited under anoxic conditions characterized by high organic carbon contents (Fig. 2q) and grayish-green colors. This is in line with the notion that intensive dissolution is generally related to anoxic conditions in organic rich sediments (Karlin and Levi, 1983, 1985; Karlin et al., 1987; Snowball, 1993; Nowaczyk et al., 2001). Third, in line with the co-occurrence of magnetite dissolution and Fe-sulfide formation (Berner, 1981, 1984; Karlin and Levi, 1983; Roberts, 1995; Rowan and Roberts, 2006; Rowan et al., 2009), pyrite is identified in the low-magnetic unit sample DCL028 but not in the high-magnetic unit sample DCL050 (Fig. 4). Fourth, in contrast with the prominent dissolution in the low-magnetic units, the high-magnetic units undergo little magnetic mineral dissolution and have a much broader magnetic grain-size distribution (including SP, SD, PSD and MD particles) and a larger average grain size than the low-magnetic units (which are dominated by PSD particles with a marginal contribution from SP, SD and MD particles) (Figs. 6 and 9). This dissolution model is illustrated by the cartoon in Fig. 10.

Pronounced reductive dissolution of magnetite is generally accompanied by less severe hematite dissolution. Consistent with this expectation, low-magnetic units have a positive linear correlation between hematite and magnetite contents (Fig. 3a, b) and an overall decrease of hematite grain size as indicated by lower L-ratios (Fig. 2h). Positive linear correlation between the L-ratio and HIRM* for the low-magnetic units (Fig. 3d) is consistent with decreasing hematite grain sizes and concentrations when dissolution intensity increases. A similar linear correlation between the L-ratio and HIRM has been applied to characterize the reductive dissolution of hematite in the eastern Mediterranean Sea sapropel layers (Liu et al. 2007). A magnetic mineralogy with relatively enhanced hematite contributions remains in the low-magnetic unit samples, which are characterized by low S^*-ratios, strongly wasp-waisted hysteresis loops and unsaturated IRM at 1 T. This supports the view that natural hematite is more resistant to reductive dissolution than magnetite (Snowball, 1993; Nowaczyk et al., 2002; Larrasoaña et al., 2003a,b; Liu et al., 2004; Demory et al., 2005).

For the high-magnetic units, the relationship between hematite and magnetite contents is scattered (Fig. 3a–c). Magnetite concentrations linearly increase with increasing magnetic grain size and detrital input (Fig. 3e, f). These observations indicate that the high-magnetic units are little affected by dissolution and that their magnetite concentration is primarily controlled by detrital input. In contrast, for the low-magnetic units, magnetite concentration is no longer

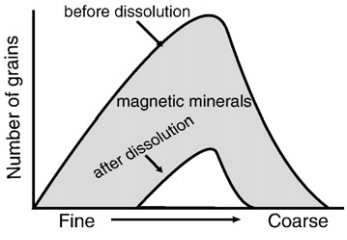

Fig. 10. Illustration of the impact of dissolution on detrital magnetic minerals in the Nihewan fluvio-lacustrine sequence.

linearly dependent on the magnetic grain size (Fig. 3e) or detrital input (Fig. 3f), and there appears to be a linear correlation between hematite and magnetite contents (Fig. 3a–c). These observations are consistent with a magnetic mineralogy that is primarily controlled by dissolution rather than detrital input.

Since dissolution of detrital magnetic minerals has resulted in concentration variations for the magnetic minerals spanning over two orders of magnitude, the Nihewan sediments therefore do not meet the criteria for yielding reliable paleointensity information (Tauxe, 1993). Thus, normalized NRM records from Nihewan fluvio-lacustrine sequences should not be interpreted in terms of geomagnetic field intensity variations. In addition, none of geomagnetic excursions that have been documented during the Brunhes Chron has been observed in the Nihewan fluvio-lacustrine sequences (Løvlie et al., 2001; Zhu et al., 2001, 2004; Wang et al., 2004, 2005; Deng et al., 2006, 2007, 2008; Li et al., 2008). This may result from fairly prolonged post-depositional remanent magnetization (PDRM) lock-in within relatively slowly deposited sediments (Roberts and Winklhofer, 2004).

6.2. Paleoclimatic significance

Major changes in the magnetic and bulk grain-size records of the Nihewan fluvio-lacustrine sequences have been suggested to correlate with glacial/interglacial cycles (Li et al., 2008; Wang et al., 2008), which implies that global climate change may be the principal mechanism driving the magnetic-property variations at Nihewan. The Xiaodukou section (Fig. 1c), which lies ~1 km west of the Xiantai section, was located at the center of the ancient lake and therefore deposited the most lacustrine sediments. According to Li et al. (2008), the χ cycles at Xiaodukou match well with bulk grain-size cycles. High-magnetic units generally contain a higher proportion of coarse-grained sediments (e.g. silts and sands) with features that indicate low lake levels, while low-magnetic units have the opposite relationship. Warm interglacial climates with high lake levels and cold glacial climates with low lake levels are most likely to have given rise to deposition of fine-grained and coarse-grained sediments, respectively. Therefore, units characterized by low χ and fine bulk grain size are correlated to interglacial periods, whereas units characterized by high χ and coarse bulk grain size are correlated to glacial periods (Li et al., 2008). This inferred relationship between magnetic mineralogy and climate is a direct follow-up of our dissolution model. Dissolution is most likely to occur during interglacial periods, when organic matter and microbial activity are more abundant, leading to anoxic diagenetic conditions and magnetic mineral dissolution in the sediments (Karlin and Levi, 1983; Thouveny et al., 1994; Williams et al., 1996). In contrast, magnetic mineral dissolution is considerably less prone to occur during the glacial periods, which implies (much) better preservation of detrital magnetic minerals. Similar mechanisms for magnetic-property changes and their relationship with climate have been reported for Lac du Bouchet, France (Thouveny et al., 1994; Williams et al., 1996).

Wang et al. (2008) explained the magnetic-property contrast between high- and low-magnetic units of the Xujiayao section on the western margin of the Nihewan Basin with a run-off model. In this model, strong runoff is interpreted to have occurred during interglacial periods, which increased the input of detrital magnetic minerals and resulted in magnetic mineral enhancement. This scenario is not applicable for (at least) the fluvio-lacustrine sequences in the eastern Nihewan Basin, as suggested by our combined magnetic and geochemical study. However, the Xujiayao section is ~60 km away from the Xiantai section (Fig. 1c), and there could exist significant spatial and temporal variations in erosion, accumulation and lithology across the Nihewan Basin. We therefore cannot conclude currently that our model is applicable to the Xujiayao area. Further research is needed to test whether the relationship between magnetic properties and climate varies across the Nihewan Basin. However, at least in the eastern area, where plentiful mammalian faunas and Paleolithic sites have been found and the classical Nihewan Formation is located, large oscillations in the magnetic mineral content are suggested to respond to glacial/interglacial cycles mainly via a dissolution/preservation process.

6.3. Implications for early human evolution in North China

The inferred relationship between magnetic properties and climate in the eastern Nihewan Basin provides valuable information on the climatic context for Paleolithic sites in this area. Both the Xiantai (1.36 Ma) and Xiaochangliang (1.36 Ma, ~200 m northeast of the Xiantai) Paleolithic sites (Fig. 1c) are found in low-magnetic units (Zhu et al., 2001; Deng et al., 2006). Human occupation at these two sites is therefore inferred to have occurred during a warm interglacial period. This interpretation is consistent with the presence of *Cervus* and *Gazella* faunal remains in the Xiaochangliang site (Zhu et al., 2001), which do not imply a cold climate. The Donggutuo site (1.1 Ma, ~1 km northeast of the Xiantai section) (Fig. 1c), which is the most extensively excavated site in the basin, spans both low- and high-magnetic units (Wang et al., 2005), and therefore represents both interglacial and glacial periods. This implies that early humans were able to resist cold glacial climate at 40°N in North China since 1.1 Ma, which is considerably earlier than the currently argued based on the glacial occupation at Zhoukoudian with an age of ~0.8 Ma (Shen et al., 2009). It is also far earlier than the ~0.5 Ma glacial occupation in Europe (Roebroeks, 1994). In addition, human occupation at the Maliang site (0.8 Ma) corresponds to high-magnetic grayish-yellow fine-grained sand layers (Wang et al., 2005), which also correlates to a cold glacial period.

7. Conclusions

Combined mineral-magnetic and geochemical data provide evidence that large-amplitude alternations of magnetic properties between high-magnetic and low-magnetic units of the Nihewan fluvio-lacustrine sequences, at least in the eastern basin, mainly result from preservation/dissolution cycles of detrital magnetic minerals in alternating oxic and anoxic depositional environments. Our preservation/dissolution model provides a basis for understanding the link between climate and magnetic properties; i.e., high- and low-magnetic units represent glacial and interglacial deposits respectively. This relationship between magnetic properties and climate provides valuable information on the climatic context for Paleolithic sites in the eastern basin. According to this relationship, early humans occupied the Xiantai and Xiaochangliang sites during an interglacial period, during both interglacial and glacial periods at Donggutuo, and during a glacial period at Maliang.

Acknowledgements

We are grateful to the Editor, Prof. Peter deMenocal, to Prof. Andrew P. Roberts and Dr. Yong-Xiang Li for their insightful comments to improve the manuscript. We also thank Profs. Jian Liu, Carlo Laj and Catherine Kissel for their insightful suggestions. This study was supported by the National Natural Science Foundation of China grant 40821091, the Ministry of Science and Technology of China (grant 2007FY110200) and the Chinese Academy of Sciences. Q. S. Liu was partly supported by the 100 Talent Program of the Chinese Academy of Sciences.

Appendix A. Supplementary data

Supplementary data associated with this article can be found, in the online version, at doi:10.1016/j.epsl.2010.01.035.

References

Ao, H., Dekkers, M.J., Deng, C.L., Zhu, R.X., 2009. Paleoclimatic significance of the Xiantai fluvio-lacustrine sequence in the Nihewan Basin (North China), based on rock magnetic properties and clay mineralogy. Geophys. J. Int. 177, 913–924.

Beaudoin, A., 2003. A comparison of two methods for estimating the organic content of sediments. J. Paleolimn. 29, 387–390.

Berner, R.A., 1981. A new geochemical classification of sedimentary environments. J. Sed. Petrol. 51, 359–365.

Berner, R.A., 1984. Sedimentary pyrite formation: an update. Geochim. Cosmochim. Acta. 48, 605–615.

Canfield, D.E., Berner, R.A., 1987. Dissolution and pyritization of magnetite in anoxic marine sediments. Geochim. Cosmochim. Acta 51, 645–659.

Carvallo, C., Muxworthy, A.R., Dunlop, D.J., 2006. First-order reversal curve (FORC) diagrams of magnetic mixtures: micromagnetic models and measurements. Phys. Earth Planet. Inter. 154, 308–322.

Chevallier, R., Mathieu, S., 1943. Proprietes magnetiques des poudres d'hematite-influence des dimensions des grains. Annales Phys. 18, 258–288.

Coey, J.M.D., 1988. Magnetic Properties of Soil Iron Oxides and Clay Minerals. Reidel Publishing, Dordrecht.

Day, R., Fuller, M., Schmidt, V.A., 1977. Hysteresis properties of titanomagnetites: grain size and composition dependence. Phys. Earth Planet. Inter. 13, 260–267.

Demory, F., Oberhansli, H., Nowaczyk, N.R., Gottschalk, M., Wirth, R., Naumann, R., 2005. Detrital input and early diagenesis in sediments from Lake Baikal revealed by rock magnetism. Glob. Planet. Change 46, 145–166.

Deng, C.L., Wei, Q., Zhu, R.X., Wang, H.Q., Zhang, R., Ao, H., Chang, L., Pan, Y.X., 2006. Magnetostratigraphic age of the Xiantai Paleolithic site in the Nihewan Basin and implications for early human colonization of Northeast Asia. Earth Planet. Sci. Lett. 244, 336–348.

Deng, C.L., Xie, F., Liu, C.C., Ao, H., Pan, Y.X., Zhu, R.X., 2007. Magnetochronology of the Feiliang Paleolithic site in the Nihewan Basin and implications for early human adaptability to high northern latitudes in East Asia. Geophys. Res. Lett. 34, L14301. doi:10.1029/2007GL030335.

Deng, C.L., Zhu, R.X., Zhang, R., Ao, H., Pan, Y.X., 2008. Timing of the Nihewan formation and faunas. Quat. Res. 69, 77–90.

Dunlop, D.J., 2002. Theory and application of the Day plot (M_{rs}/M_s versus H_{cr}/H_c) 1. Theoretical curves and tests using titanomagnetite data. J. Geophys. Res. 107. doi:10.1029/2001JB000486.

Dunlop, D.J., Özdemir, Ö., 1997. Rock Magnetism: Fundamentals and Frontiers. Cambridge University Press, Cambridge (UK).

Evans, M.E., Heller, F., 2003. Environmental Magnetism: Principles and Applications of Enviromagnetics. Academic Press, Oxford.

Karlin, R., Levi, S., 1983. Diagenesis of magnetic minerals in recent hemipelagic sediments. Nature 303, 327–330.

Karlin, R., Levi, S., 1985. Geochemical and sedimentological control of the magnetic properties of hemipelagic sediments. J. Geophys. Res. 90, 373–392.

Karlin, R., Lyle, M., Heath, G.R., 1987. Authigenic magnetite formation in suboxic marine sediments. Nature 326, 490–493.

Kosterov, A., 2003. Low-temperature magnetization and AC susceptibility of magnetite: effect of thermomagnetic history. Geophys. J. Int. 154, 58–71.

Larrasoaña, J.C., Roberts, A.P., Stoner, J.S., Richter, C., Wehausen, R., 2003a. A new proxy for bottom-water ventilation in the eastern Mediterranean based on diagenetically controlled magnetic properties of sapropel-bearing sediments. Palaeogeogr. Palaeoclimatol. Palaeoecol. 190, 221–242.

Larrasoaña, J.C., Roberts, A.P., Rohling, E.J., Winklhofer, M., Wehausen, R., 2003b. Three million years of monsoon variability over the northern Sahara. Clim. Dyn. 21, 689–698.

Li, H.M., Yang, X.Q., Heller, F., Li, H.T., 2008. High resolution magnetostratigraphy and deposition cycles in the Nihewan Basin (North China) and their significance for stone artifact dating. Quat. Res. 69, 250–262.

Liu, J., Zhu, R.X., Roberts, A.P., Li, S.Q., Chang, J.H., 2004. High-resolution analysis of early diagenetic effects on magnetic minerals in post-middle-Holocene continental shelf sediments from the Korea Strait. J. Geophys. Res. 109, B03103. doi:10.1029/2003JB002813.

Liu, Q.S., Roberts, A.P., Torrent, J., Horng, C.S., Larrasoaña, J.C., 2007. What do the HIRM and S-ratio really measure in environmental magnetism? Geochem. Geophys. Geosyst. 8, Q09011. doi:10.1029/2007GC001717.

Løvlie, R., Su, P., Fan, X.Z., Zhao, Z.J., Liu, C., 2001. A revised paleomagnetic age of the Nihewan Group at the Xujiayao Palaeolithic Site. China. Quat. Sci. Rev. 20, 1341–1353.

Moskowitz, B.M., Frankel, R.B., Bazylinski, D.A., 1993. Rock magnetic criteria for the detection of biogenic magnetite. Earth Planet. Sci. Lett. 120, 283–300.

Moskowitz, B.M., Jackson, M., Kissel, C., 1998. Low-temperature magnetic behavior of titanomagnetites. Earth Planet. Sci. Lett. 157, 141–149.

Muxworthy, A.R., Dunlop, D.J., 2002. First-order reversal curve (FORC) diagrams for pseudo-single-domain magnetites at high temperature. Earth Planet. Sci. Lett. 203, 369–382.

Nowaczyk, N.R., Harwart, S., Melles, M., 2001. Impact of early diagenesis and bulk particle grain size distribution on estimates of relative geomagnetic palaeointensity variations in sediments from Lama Lake, northern Central Siberia. Geophys. J. Int. 145, 300–306.

Nowaczyk, N.R., Minyuk, P., Melles, M., Brigham-Grette, J., Glushkova, O., Nolan, M., Lozhkin, A.V., Stetsenko, T.V., Andersen, P.M., Forman, S.L., 2002. Magnetostratigraphic results from impact crater Lake El'gygytgyn, northeastern Siberia: a 300 kyr long high-resolution terrestrial palaeoclimatic record from the Arctic. Geophys. J. Int. 150, 109–126.

Ortega, B., Caballero, M., Lozano, S., Vilaclara, G., Rodriguez, A., 2006. Rock magnetic and geochemical proxies for iron mineral diagenesis in a tropical lake: Lago Verde, Los Tuxtlas. East-Central Mexico. Earth Planet. Sci. Lett. 250, 444–458.

Passier, H.F., Dekkers, M.J., 2002. Iron oxide formation in the active oxidation front above sapropel S1 in the eastern Mediterranean Sea as derived from low-temperature magnetism. Geophys. J. Int. 150, 230–240.

Pei, S.W., 2002. The Paleolithic site at Dachangliang in the Nihewan Basin, north China (in Chinese with English abstract). Acta Anthropol. Sinica 21, 116–125.

Pike, C.R., Roberts, A.P., Verosub, K.L., 2000. The effect of magnetic interactions on low temperature saturation remanence in fine magnetic particle systems. J. Appl. Phys. 88, 967–974.

Pike, C.R., Roberts, A.P., Verosub, K.L., 2001. First-order reversal curve diagrams and thermal relaxation effects in magnetic particles. Geophy. J. Int. 145, 721–730.

Roberts, A.P., 1995. Magnetic properties of sedimentary Greigite (Fe_3S_4). Earth Planet. Sci. Lett. 134, 227–236.

Roberts, A.P., Cui, Y.L., Verosub, K.L., 1995. Wasp-waisted hysteresis loops: mineral magnetic characteristics and discrimination of components in mixed magnetic systems. J. Geophys. Res. 100, 17909–17924.

Roberts, A.P., Winklhofer, M., 2004. Why are geomagnetic excursions not always recorded in sediments? Constraints from post-depositional remanent magnetization lock-in modelling. Earth Planet. Sci. Lett. 227, 345–359.

Roberts, A.P., Pike, C.R., Verosub, K.L., 2000. First-order reversal curve diagrams: a new tool for characterizing the magnetic properties of natural samples. J. Geophys. Res. 105, 28461–28475.

Roebroeks, W., 1994. Updating the earliest occupation of Europe. Curr. Anthrop. 35, 301–305.

Rosenbaum, J.G., Reynolds, R.L., Adam, D.P., Drexler, J., Sarna-Wojcicki, A.M., Whitney, G.C., 1996. Record of middle Pleistocene climate change from Buck Lake, Cascade Range, southern Oregon—evidence from sediment magnetism, trace-element geochemistry, and pollen. Geol. Soc. Am. Bull. 108, 1328–1341.

Rowan, C.J., Roberts, A.P., 2006. Magnetite dissolution, diachronous greigite formation, and secondary magnetizations from pyrite oxidation: unravelling complex magnetizations in Neogene marine sediments from New Zealand. Earth Planet. Sci. Lett. 241, 119–137.

Rowan, C.J., Roberts, A.P., Broadbent, T., 2009. Reductive diagenesis, magnetite dissolution, greigite growth and paleomagnetic smoothing in marine sediments: A new view. Earth Planet. Sci. Lett. 277, 223–235.

Shen, G.J., Gao, X., Granger, D.E., 2009. Age of Zhoukoudian *Homo erectus* determined with $^{26}Al/^{10}Be$ burial dating. Nature 458, 198–200.

Snowball, I.F., 1993. Geochemical control of magnetite dissolution in subarctic lake sediments and the implications for environmental magnetism. J. Quat. Sci. 8, 339–346.

Tarduno, J.A., 1994. Temporal trends of magnetic dissolution in the pelagic realm: gauging paleoproductivity? Earth Planet. Sci. Lett. 123, 39–48.

Tarduno, J.A., 1995. Superparamagnetism and reduction diagenesis in pelagic sediments: enhancement or depletion. Geophys. Res. Lett. 22, 1337–1340.

Tauxe, L., 1993. Sedimentary records of relative paleointensity of the geomagnetic field: theory and practice. Rev. Geophys. 31, 319–354.

Thompson, R., Bloemendal, J., Dearing, J.A., Oldfield, F., Rummery, T.A., Stober, J.C., Turner, G.M., 1980. Environmental applications of magnetic measurements. Science 207, 481–486.

Thouveny, N., Debeaulieu, J.L., Bonifay, E., Creer, K.M., Guiot, J., Icole, M., Johnsen, S., Jouzel, J., Reille, M., Williams, T., Williamson, D., 1994. Climate variations in Europe over the past 140-kyr deduced from rock magnetism. Nature 371, 503–506.

Wang, X.S., Yang, Z.Y., Løvlie, R., Min, L.R., 2004. High-resolution magnetic stratigraphy of fluvio-lacustrine succession in the Nihewan Basin. China. Quat. Sci. Rev. 23, 1187–1198.

Wang, H.Q., Deng, C.L., Zhu, R.X., Wei, Q., Hou, Y.M., Boëda, E., 2005. Magnetostratigraphic dating of the Donggutuo and Maliang Paleolithic sites in the Nihewan Basin, North China. Quat. Res. 64, 1–11.

Wang, X.S., Løvlie, R., Su, P., Fan, X.Z., 2008. Magnetic signature of environmental change reflected by Pleistocene lacustrine sediments from the Nihewan Basin, North China. Palaeogeogr. Palaeoclimatol. Palaeoecol. 260, 452–462.

Williams, T., Thouveny, N., Creer, K.M., 1996. Palaeoclimatic significance of the 300 ka mineral magnetic record from the sediments of Lac du Bouchet. France. Quat. Sci. Rev. 15, 223–235.

Williamson, D., Jelinowska, A., Kissel, C., Tucholka, P., Gibert, E., Gasse, F., Massault, M., Taieb, M., Van Campo, E., Wieckowski, K., 1998. Mineral-magnetic proxies of erosion/oxidation cycles in tropical maar-lake sediments (Lake Tritrivakely, Madagascar): paleoenvironmental implications. Earth Planet. Sci. Lett. 155, 205–219.

Worm, H.U., 1998. On the superparamagnetic-stable single domain transition for magnetite, and frequency dependence of susceptibility. Geophys. J. Int. 133, 201–206.

Zhu, R.X., Hoffman, K.A., Potts, R., Deng, C.L., Pan, Y.X., Guo, B., Shi, C.D., Guo, Z.T., Yuan, B.Y., Hou, Y.M., Huang, W.W., 2001. Earliest presence of humans in northeast Asia. Nature 413, 413–417.

Zhu, R.X., Potts, R., Xie, F., Hoffman, K.A., Deng, C.L., Shi, C.D., Pan, Y.X., Wang, H.Q., Shi, R.P., Wang, Y.C., Shi, G.H., Wu, N.Q., 2004. New evidence on the earliest human presence at high northern latitudes in northeast Asia. Nature 431, 559–562.

Zhu, R.X., Deng, C.L., Pan, Y.X., 2007. Magnetochronology of the fluvio-lacustrine sequences in the Nihewan basin and its implications for early human colonization of Northeast Asia (in Chinese with English abstract). Quat. Sci. 27 (6), 922–944.